Tokyo Climate Center, Japan Meteorological Agency

TCC News

No. 42 Autumn 2015

Contents

El Niño Outlook (October 2015 – April 2016)

It is likely that El Niño conditions will continue until boreal spring 2016. (This article was written based on El Nino outlook issued on 9 October 2015.)

El Niño/La Niña

In September 2015, the NINO.3 sea surface temperature (SST) was above normal with a deviation of +2.6°C, which is the second-highest value for September since 1950. The five-month running mean of the NINO.3 SST deviation was +0.5°C or above for 14 consecutive months ending in July. SSTs (Figures 1 and 3 (a)) were remarkably above normal from near the date line to the South American coast over the equatorial Pacific. Subsurface temperatures (Figures 2 and 4 (b)) were below normal in the western equatorial Pacific and remarkably above normal in the central and eastern parts. Atmospheric convective activity was significantly above normal from near the date line to the central equatorial Pacific, and easterly winds in the lower troposphere (known as trade winds) were remarkably below normal in the central part. These oceanic and atmospheric characteristics indicate that El Niño conditions remain ongoing in the equatorial Pacific.

The subsurface warm waters observed in September in the equatorial Pacific are expected to support the maintenance of warmer-than-normal SST conditions in its eastern part in the months ahead. JMA's El Niño prediction model indicates that the NINO.3 SST will be above normal until boreal spring (Figure 4). In conclusion, El Niño conditions are likely to continue until boreal spring.

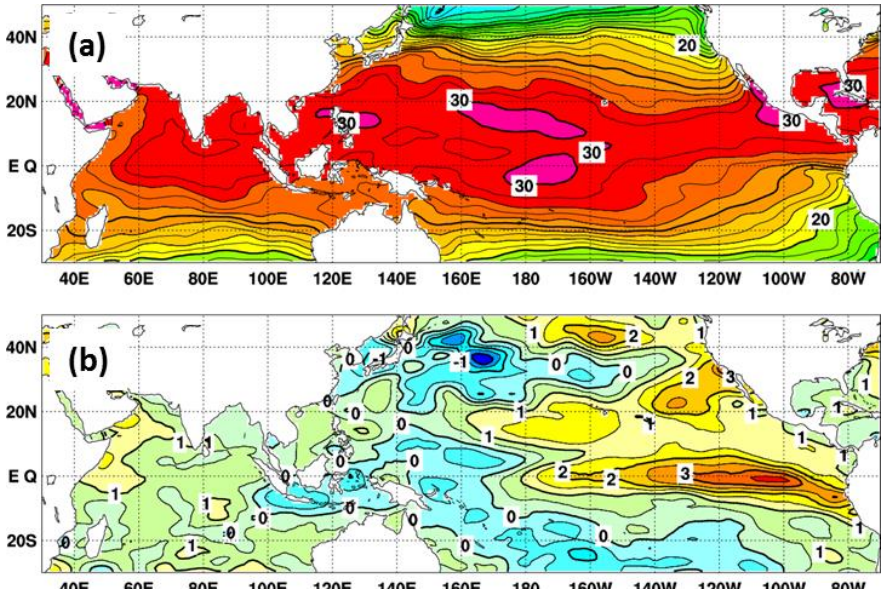

Figure 1
Monthly mean (a) sea surface temperatures (SSTs) and (b) SST anomalies in the Indian and Pacific Ocean areas for September 2015
The contour intervals are 1˚C in (a) and 0.5˚C in (b). The base period for the normal is 1981 – 2010.

Western Pacific and Indian Ocean

The area-averaged SST for the tropical western Pacific (NINO.WEST) region was below normal in September, and is likely to generally remain below normal until boreal spring.

The area-averaged SST for the tropical Indian Ocean (IOBW) region was above normal in September, and is likely to remain above normal until boreal spring.

Impacts

In September 2015, the cooler-than-normal conditions observed in Eastern Japan and Western Japan, were consistent with patterns commonly seen in past El Niño events.

In the same month, warmer-than-normal conditions in India and the northern part of South America, and drier-than-normal conditions in the northern part of South America were consistent with patterns commonly seen in past El Niño events.

(Ikuo Yoshikawa, Climate Prediction Division)

* The SST normal for NINO.3 region (5°S – 5°N, 150°W – 90°W) is defined as an monthly average over a sliding 30-year period (1985-2014 for this year).

* The SST normals for the NINO.WEST region (Eq. – 15°N, 130°E – 150°E) and the IOBW region (20°S – 20°N, 40°E – 100°E) are defined as linear extrapolations with respect to a sliding 30-year period, in order to remove the effects of significant long-term warming trends observed in these regions.

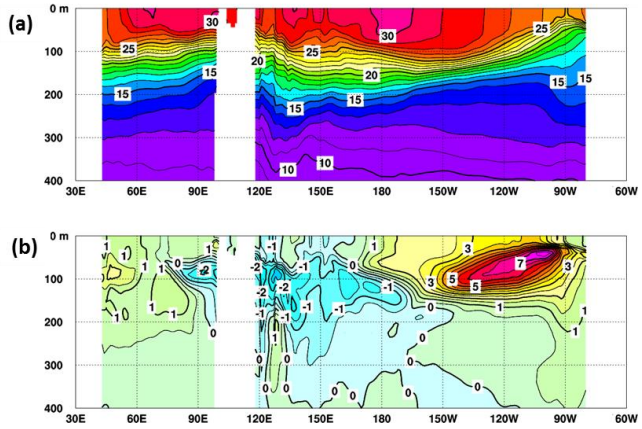

Figure 2 Monthly mean depth-longitude cross sections of (a) temperatures and (b) temperature anomalies in the equatorial Indian and Pacific Ocean areas for September 2015
The contour intervals are 1˚C in (a) and 0.5˚C in (b). The base period for the normal is 1981 – 2010.

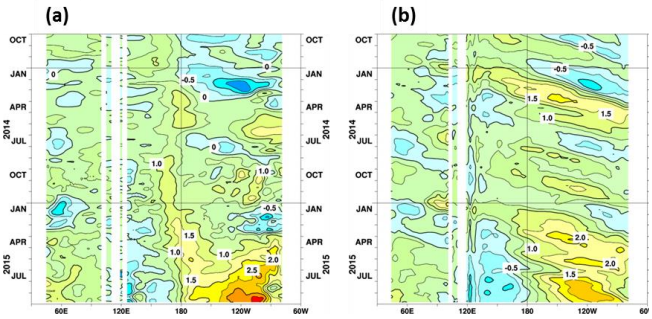

Figure 3 Time-longitude cross sections of (a) SST and (b) ocean heat content (OHC) anomalies along the equator in the Indian and Pacific Ocean areas
OHCs are defined here as vertical averaged temperatures in the top 300 m. The base period for the normal is 1981 – 2010.

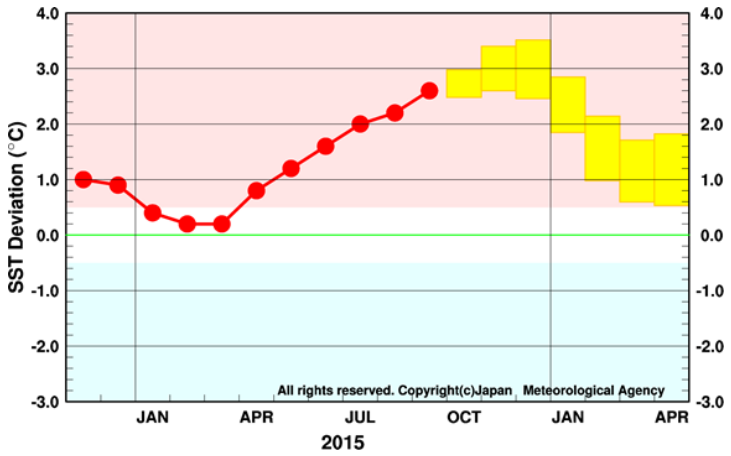

Figure 4 Outlook of NINO.3 SST deviation produced by the El Niño prediction model
This figure shows a time series of monthly NINO.3 SST deviations. The thick line with closed circles shows observed SST deviations, and the boxes show the values produced for the next six months by the El Niño prediction model. Each box denotes the range into which the SST deviation is expected to fall with a probability of 70%.

JMA's Seasonal Numerical Ensemble Prediction for Boreal Winter 2015/2016

Based on JMA's seasonal ensemble prediction system, sea surface temperature (SST) anomalies are predicted to be above normal in the central and eastern equatorial Pacific during this boreal winter, suggesting a continuation of El Niño conditions. In association with El Niño conditions, active convection is predicted over the central equatorial Pacific. Conversely, inactive convection is predicted over most of the Maritime Continent. Additionally, the Aleutian Low is predicted to be located northeast of its normal position.

1. Introduction

This article outlines JMA's dynamical seasonal ensemble prediction for boreal winter 2015/2016 (December – February, referred to as DJF), which was used as a basis for the Agency's operational warm-season outlook issued on 23 October 2015. The outlook detailed here is based on the seasonal ensemble prediction system of the Coupled Atmosphere-ocean General Circulation Model (CGCM). See the column below for system details.

Section 2 outlines global SST anomaly predictions, and Section 3 describes the associated circulation field predictions for the tropics and sub-tropics. Finally, the circulation fields predicted for the mid- and high latitudes of the Northern Hemisphere are discussed in Section 4.

2. SST anomalies (Figure 5)

Figure 5 shows predicted SSTs (contours) and related anomalies (shading) for DJF. Above normal anomalies are predicted in the central and eastern equatorial Pacific Ocean throughout the period, suggesting a continuation of El Niño conditions. Above normal anomalies are also predicted in the Indian Ocean. Conversely, slightly below-normal anomalies are predicted in the Philippine Sea.

3. Prediction for the tropics and sub-tropics (Figure 6)

Figure 6 (a) shows predicted precipitation (contours) and related anomalies (shading) for DJF. In association with the ongoing El Niño conditions, above-normal anomalies are predicted over the central equatorial Pacific Ocean. Conversely, below-normal anomalies are predicted over most of the Maritime Continent.

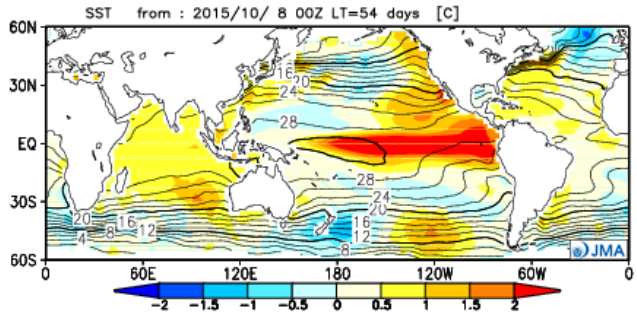

Figure 5 Predicted SSTs (contours) and SST anomalies (shading) for December–February 2015/2016 (ensemble mean of 51 members)

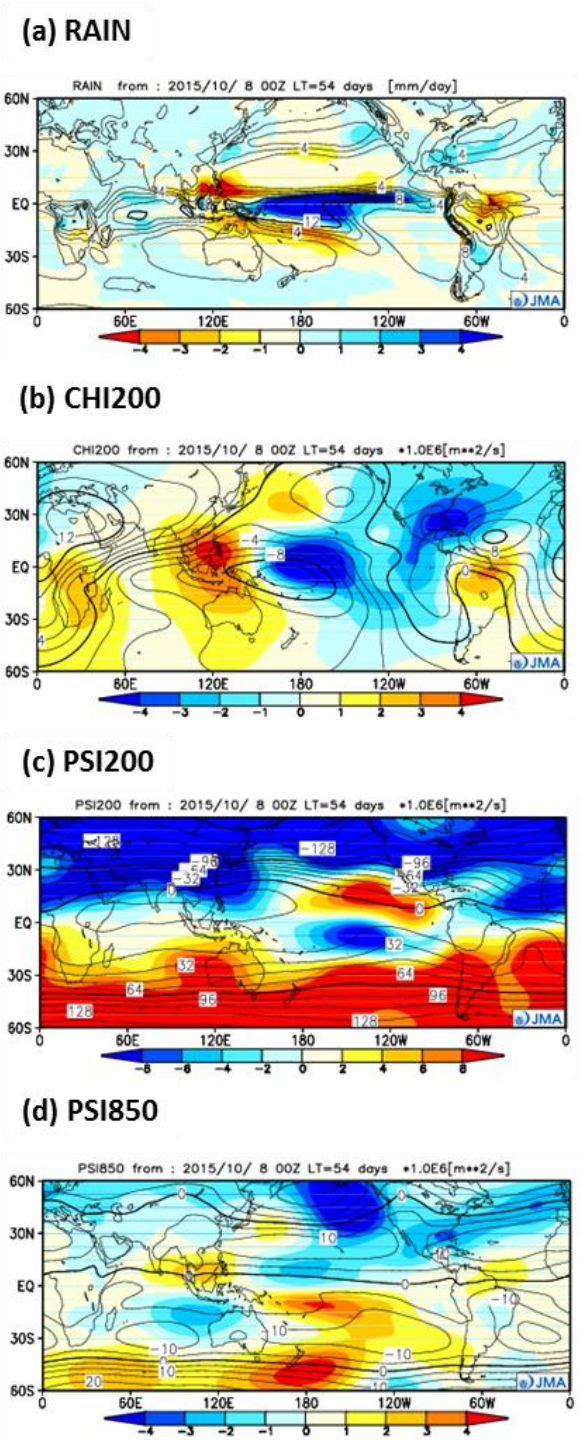

Figure 6 Predicted atmospheric fields from 60°N – 60°S for December–February 2015/2016 (ensemble mean of 51 members)

(a) Precipitation (contours) and anomaly (shading). The contour interval is 2 mm/day.

(b) Velocity potential at 200 hPa (contours) and anomaly (shading). The contour interval is 2×10^6 m^2/s.

(c) Stream function at 200 hPa (contours) and anomaly (shading). The contour interval is 16×10^6 m^2/s.

(d) Stream function at 850 hPa (contours) and anomaly (shading). The contour interval is 5×10^6 m^2/s.

Figure 6 (b) shows predicted velocity potential (contours) and related anomalies (shading) at the upper troposphere (200 hPa) for DJF. Negative (i.e., divergent) anomalies are predicted over the central equatorial Pacific, reflecting active convection. Conversely, positive (i.e., convergent) anomalies are predicted over the Maritime Continent, reflecting inactive convection.

Figure 6 (c) shows predicted stream functions (contours) and related anomalies (shading) at the upper troposphere (200 hPa) for DJF. Negative anomalies are predicted for most of the Northern Hemisphere, suggesting a southward-shifting tendency of subtropical jet stream. Moreover, equatorial symmetric anticyclonic anomalies are predicted around the central equatorial Pacific as a response from active convection. Conversely, equatorial symmetric cyclonic anomalies are predicted around the Maritime Continent as a response from inactive convection.

Figure 6 (d) shows predicted stream functions (contours) and related anomalies (shading) at the lower troposphere (850 hPa) for DJF. Equatorial symmetric cyclonic anomalies are predicted around the central equatorial Pacific as a response from active convection. Conversely, equatorial symmetric anticyclonic anomalies are predicted around the Maritime Continent as a response from inactive convection.

4. Prediction for the mid- and high- latitudes of the Northern Hemisphere (Figure 7)

Figure 7 (a) shows predicted geopotential heights (contours) and related anomalies (shading) at 500 hPa for DJF. Positive anomalies are predicted over most of the Northern Hemisphere, reflecting El Niño conditions and a recent trend of global warming. However, negative anomalies are predicted over the northeastern part of the North Pacific and the southern part of North America in association with the Pacific North American (PNA) teleconnection pattern often observed in El Niño winters.

Figure 7 (b) shows predicted sea level pressure (contours) and related anomalies (shading) for DJF. Negative anomalies are predicted over the northeastern part of the North Pacific, while positive anomalies are predicted over its southwestern part, suggesting a northeastward shift of the Aleutian Low. Additionally, slightly negative anomalies are predicted in Siberia, suggesting a weak Siberian High. However, this should be interpreted with caution due to the relatively low skill of the prediction.

(Takashi Yamada, Climate Prediction Division)

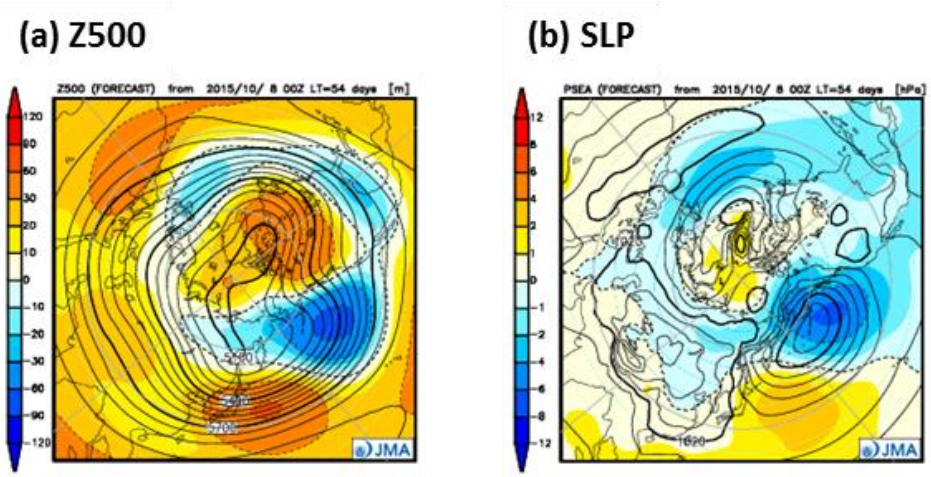

Figures 7 Predicted atmospheric fields from 20°N – 90°N for December–February 2015/2016 (ensemble mean of 51 members)
(a) Geopotential height at 500hPa (contours) and anomaly (shading). The contour interval is 60 m.
(b) Sea level pressure (contours) and anomaly (shading). The contour interval is 4hPa.

JMA's Seasonal Ensemble Prediction System

JMA operates a seasonal Ensemble Prediction System (EPS) using the Coupled atmosphere-ocean General Circulation Model (CGCM) to make seasonal predictions beyond a one-month time range. The EPS produces perturbed initial conditions by means of a combination of the initial perturbation method and the lagged average forecasting (LAF) method. The prediction is made using 51 members from the latest four initial dates (thirteen members are run every five days). Details of the prediction system and verification maps based on 30-year hindcast experiments (1981–2010) are available at http://ds.data.jma.go.jp/tcc/tcc/products/model/.

Cold Season Outlook for Winter 2015/2016 in Japan

In winter 2015/2016, mean temperatures are expected to be above normal in eastern Japan, western Japan and Okinawa/Amami, and near normal in northern Japan. Cold-season precipitation amounts are expected to be above normal on the Pacific side of eastern and western Japan and in Okinawa/Amami. Cold season snowfall amounts for the Sea of Japan side are expected to be below normal in eastern Japan.

1. Outlook summary (Figure 8)

JMA issued its outlook for the coming winter (December 2015 – February 2016) over Japan in September and updated it on 23 October based on the output of its seasonal Ensemble Prediction System (EPS). This article summarizes the update.

According to the outlook, mean temperatures in winter 2015/2016 will be above normal in Okinawa/Amami with 60% probability and in western and eastern Japan with 50% probability, and near normal in northern Japan. Cold-season precipitation amounts are expected to be above normal on the Pacific side of eastern and western Japan and in Okinawa/Amami with 50% probability, slightly above normal on the Sea of Japan side of western Japan with 40% probability, slightly below normal on the Sea of Japan side of eastern Japan with 40% probability, and near normal in northern Japan. Snowfall amounts for the Sea of Japan side are expected to be below normal in eastern Japan with 50% probability, slightly below normal in western Japan with 40% probability, and near normal in northern Japan.

2. Outlook background

The schematic diagram in Figure 9 shows expected large-scale ocean and atmospheric characteristics for this winter. The background to the outlook is summarized below.

* Sea surface temperatures are expected to be above normal from the date line to the eastern part of the equatorial Pacific and the Indian Ocean, and relatively low in the western tropical Pacific. Those anomaly patterns are similar to those observed in past El Niño events.
* Convection over the tropics is expected to be more active than normal from the date line to the eastern Pacific and less active than normal around the Maritime continent.
* In association with inactive convection around the Maritime continent, the subtropical jet stream is expected to meander southward around southern China and northward east of Japan.
* Accordingly, southwesterly anomalies of the upper flow are expected around Japan, which would bring a suppressed northwesterly monsoon, especially in southern part of Japan. This would enhance the likelihood of increased impacts from low pressure on the Pacific side of Japan and reduce the likelihood of snowfall from the northwesterly monsoon on the Sea of Japan side of eastern Japan.
* Higher-than-normal temperatures in the troposphere (possibly associated with the development of El Niño conditions and the prevailing long-term trend) are predicted. These tendencies are likely to increase the likelihood of above-normal temperatures, especially in the lower latitudes.

(Masayuki Hirai, Climate Prediction Division)

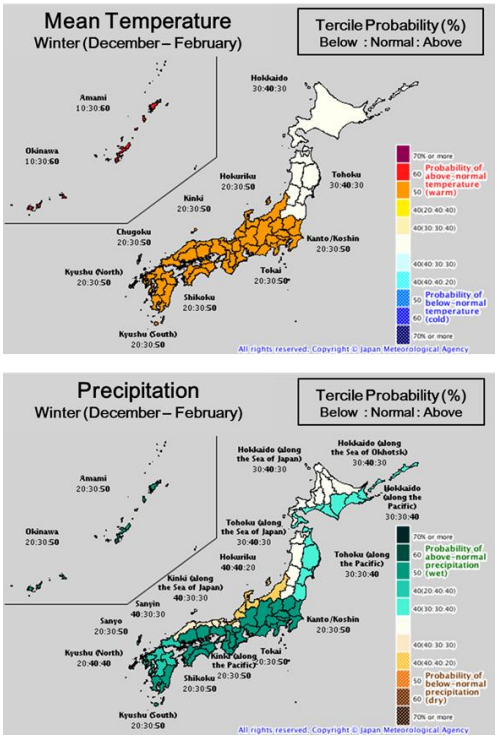

Figure 8 Outlook for winter 2015/2016 temperature (above) and precipitation (below) probability in Japan.

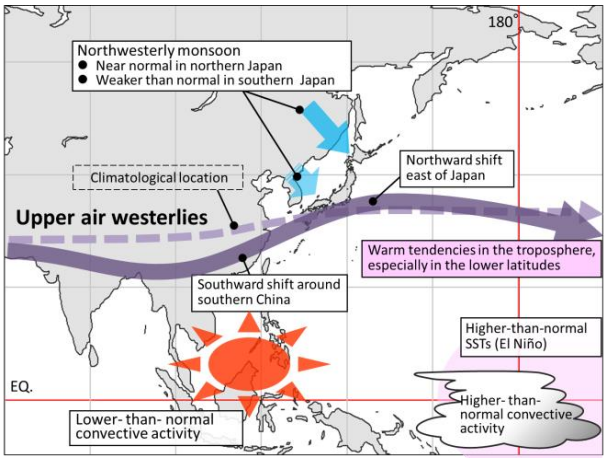

Figure 9 Schematic diagram showing expected large-scale characteristics of the ocean and atmosphere in winter 2015/16

1. Precipitation and temperature

Four-month total precipitation amounts based on CLIMAT reports during the monsoon season (June – September) were more than 140% of the normal on the Pacific side of eastern to western Japan, in eastern China, in southern Mongolia and northwestern China, and in and around Pakistan. Conversely, the corresponding figures were less than 40% of the normal around the western part of the Korean Peninsula and in southern to western Indonesia (Figure 10 (a)). These amounts were mostly consistent with the distribution of four-month mean OLR anomalies (Figure 11).

Extremely heavy precipitation was seen from Kyushu region (the most southwesterly of its four main islands of Japan) of Japan to central China in June. In contrast, extremely light precipitation was seen in Mongolia in August (figures not shown).

Four-month mean temperatures for the same period were more than 1°C above normal from the southern part of Central Siberia to northern Mongolia, on the central Korean Peninsula, on the northern Indochina Peninsula and in central and southwestern India, and were more than 1°C below normal around the middle Yangtze River basin (Figure 10 (b)).

It was reported that heavy rains often caused floods and landslides in eastern and western India and in northern and eastern Pakistan. Monsoon-season fatalities caused by floods and landslides reportedly exceeded 660 in India and 220 in Pakistan. Heat waves in June reportedly caused more than 1,220 fatalities in southwestern Pakistan.

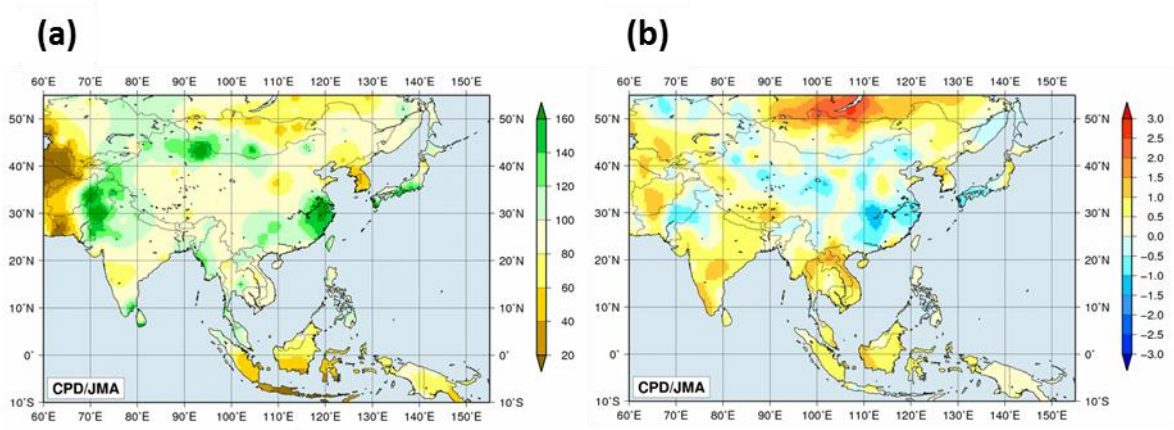

Figure 10 (a) Four-month precipitation ratios (%) from June to September 2015
(b) Four-month mean temperature anomalies (°C) from June to September 2015

The base period for normal is 1981 – 2010. There were not data in Afghanistan.

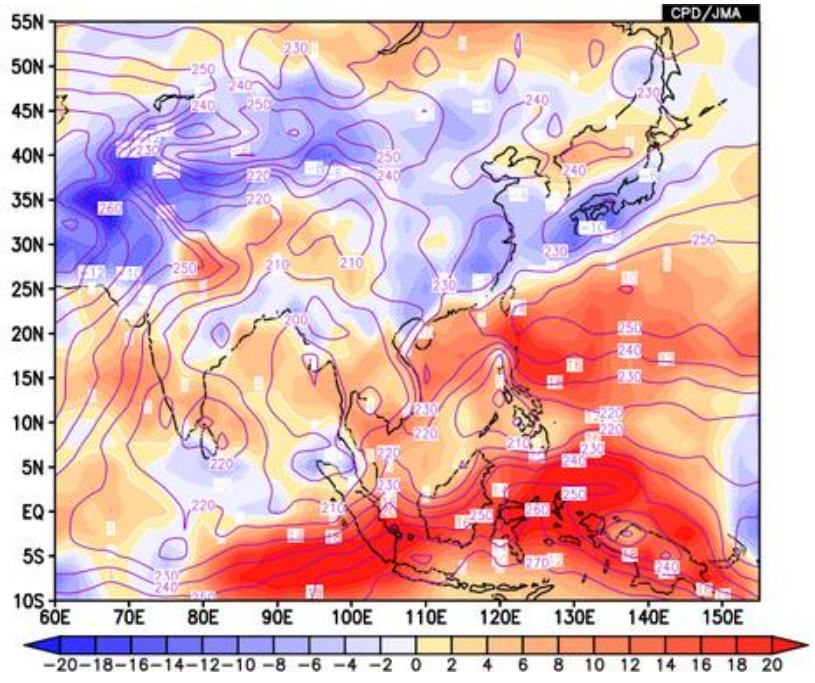

Figure 11 Four-month mean OLR and its anomaly for June–September 2015
The contours indicate OLR at intervals of 10 W/m^2, and the color shading denotes OLR anomalies from the normal (i.e., the 1981–2010 average). Negative (cold color) and positive (warm color) OLR anomalies show enhanced and suppressed convection compared to the normal, respectively. Original data are provided by NOAA.

2. Tropical cyclones

During the monsoon season, 14 tropical cyclones (TCs) of tropical storm (TS) intensity or higher formed over the western North Pacific (Table 1). This was lower than the normal (1981-2010 average) of 16.0. The average position of TC formations was south and east of the normal. Four TCs hit the main islands of Japan, which was above the annual normal of 2.7.

Fatalities from Typhoon Soudelor reportedly exceeded 20 in China, and those from Typhoon Goni reportedly exceeded 30 in the Philippines.

Note: Disaster information is based on reports by governmental organizations (China, India, Pakistan and the Philippines) and EM-DAT[*].*

[*]: D. Guha-Sapir, R. Below, Ph. Hoyois - EM-DAT: International Disaster Database - www.emdat.be - Université Catholique de Louvain - Brussels - Belgium.

Table 1 Tropical cyclones forming over the western North Pacific from June to September 2015

Number ID	Name	Date (UTC)	Category[1)]	Maximum wind[2)] (knots)
T1508	Kujira	6/21 – 6/24	TS	45
T1509	Chan-Hom	6/30 – 7/12	TY	90
T1510	Linfa	7/2 – 7/9	STS	50
T1511	Nangka	7/3 – 7/17	TY	100
T1512	Halola	7/13 – 7/16, 7/19 – 7/26	TY	80
T1513	Soudelor	8/1 – 8/9, 8/11 – 8/11	TY	115
T1514	Molave	8/7 – 8/13	TS	45
T1515	Goni	8/14 – 8/25	TY	100
T1516	Atsani	8/14 – 8/25	TY	100
T1517	Kilo	9/2 – 9/11	TY	80
T1518	Etau	9/7 – 9/9	STS	50
T1519	Vamco	9/13 – 9/14	TS	35
T1520	Krovanh	9/15 – 9/21	TY	85
T1521	Dujuan	9/22 – 9/29	TY	110

Note: Based on information from the RSMC Tokyo-Typhoon Center.
1) Intensity classification for tropical cyclones
TS: tropical storm, STS: severe tropical storm, TY: typhoon
2) Estimated maximum 10-minute mean wind

3. Monsoon activity and atmospheric circulation

Convective activity (inferred from OLR) averaged for June – September 2015 was enhanced from eastern China to eastern Japan, and was suppressed over large parts of the Asian summer monsoon region, especially over the area around the Maritime Continent and east of the Philippines (Figure 11). According to the OLR indices (Table 2), the overall activity of the Asian summer monsoon (represented by the SAMOI (A) index) was below normal throughout the summer monsoon season, especially in August.

In the upper troposphere, the Tibetan High was generally weaker than normal (Figure 12 (a)), which was consistent with the subtropical jet stream flowing southward of its normal position. In the lower troposphere, monsoon circulation over the Indian Ocean was weaker than normal and the Somali jet was weaker than normal. Zonal wind shear between the upper and lower troposphere over the North Indian Ocean and southern Asia (Figure 13) remained weaker than normal after July. The northwestward extension of the Pacific High was weaker than normal, contributing to cool wet summer conditions around western Japan (Figure 12 (b)).

(Section 1 and 2: Ayako Takeuchi, 3: Hitomi Saitou, Climate Prediction Division)

Table 2 Summer Asian Monsoon OLR Index (SAMOI) values observed from May to October 2015

Asian summer monsoon OLR indices (SAMOI) are derived from OLR anomalies from May to October. SAMOI (A), (N) and (W) indicate the overall activity of the Asian summer monsoon, its northward shift and its westward shift, respectively. SAMOI definitions are as follows: SAMOI (A) = (-1) × (W + E); SAMOI (N) = S – N; SAMOI (W) = E – W. W, E, N and S indicate area-averaged OLR anomalies for the respective regions shown in the figure on the right normalized by their standard deviations.

	Summer Asian Monsoon OLR Index (SAMOI)		
	SAMOI (A): Activity	SAMOI (N): Northward-shift	SAMOI (W): Westward-shift
May 2015	-1.2	0.4	2.0
Jun. 2015	-1.2	-1.5	0.6
Jul. 2015	-0.7	2.0	0.4
Aug. 2015	-1.9	0.2	0.6
Sep. 2015	-1.0	-0.4	1.4
Oct. 2015	-1.4	1.8	0.6

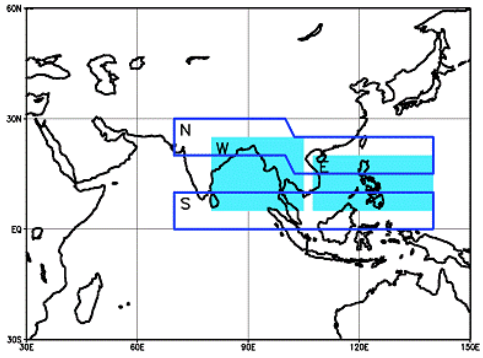

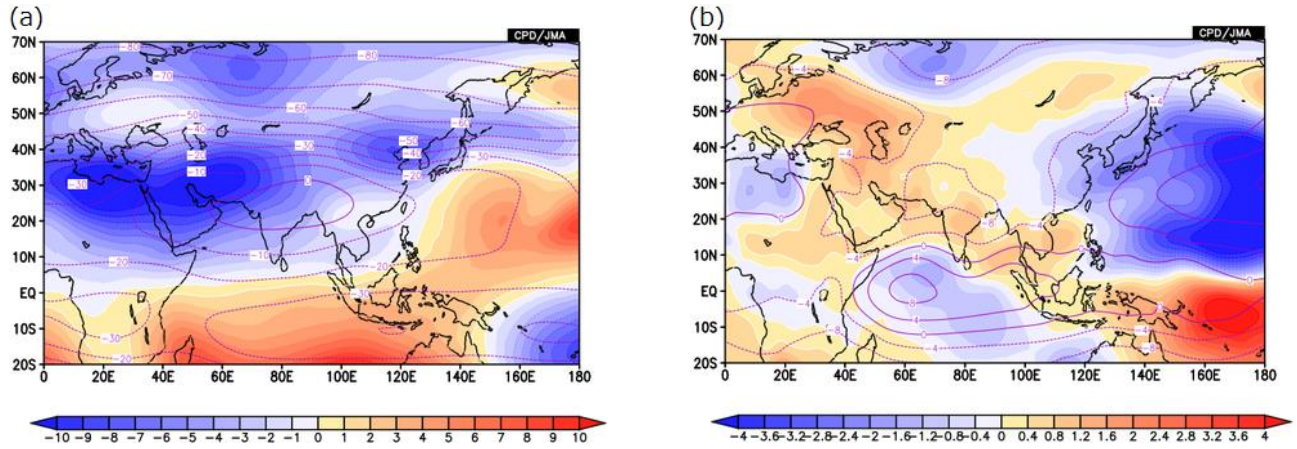

Figure 12 Four-month mean stream function and its anomaly for June – September 2015

(a) The contours indicate the 200-hPa stream function at intervals of 10×10^6 m^2/s, and the color shading indicates 200-hPa stream function anomalies from the normal. (b) The contours indicate the 850-hPa stream function at intervals of 4×10^6 m^2/s, and the color shading indicates 850-hPa stream function anomalies from the normal. The base period for the normal is 1981 – 2010. Warm (cold) shading denotes anticyclonic (cyclonic) circulation anomalies in the Northern Hemisphere, and vice-versa in the Southern Hemisphere.

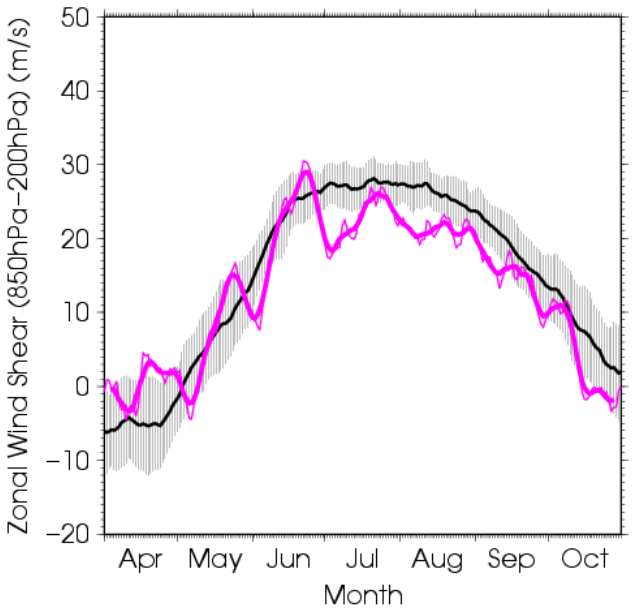

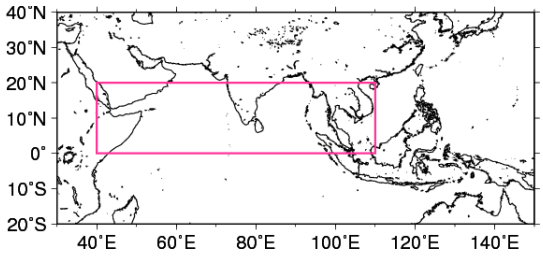

Figure 13 Time-series representation of the zonal wind shear index between 200-hPa and 850-hPa averaged over the North Indian Ocean and southern Asia (the region enclosed by the pink rectangle in the right figure: equator – 20°N, 40°E – 110°E)

The zonal wind shear index is calculated after Webster and Yang (1992). The thick and thin pink lines indicate seven-day running mean and daily mean values, respectively. The black line denotes the normal (i.e., the 1981 – 2010 average), and the gray shading shows the range of the standard deviation calculated for the time period of the normal.

References

Webster, P. J. and S. Yang, 1992: Monsoon and ENSO: Selectively interactive systems. *Quart. J. Roy. Meteor. Soc.*, **118**, 877 – 926.

The Antarctic ozone hole in 2015 was the fourth-largest since 1979.

Over the last 30 years, the Antarctic ozone hole has appeared every year in Austral spring with a peak in September or early October. It is generally defined as the area in which the total ozone column is equal to or less than 220 m atm-cm.

According to JMA's analysis based on Aura OMI data, the Antarctic ozone hole for 2015 appeared in mid-August and expanded rapidly from late August to early September, although it remained small compared to the average for the previous ten years (Figure 14 (a)). In mid-September and early October (usually a period of ozone hole contraction), the ozone hole continued to expand moderately and reached its maximum size for the year on 9 October (Figure 14 (b)). At this time it had a total area of 27.8 million square kilometers, which was twice as large as that of the Antarctic Continent. The maximum size was equivalent to that of 1998, making it the fourth-largest since 1979 (Figure 14 (c)) and the largest on record for any October (Figure 14 (d)). The expansion observed in 2015 may have been caused by a stable and large polar vortex over Antarctica because the vortex in 2015 covered a larger area over Antarctica and exhibited lower temperatures than in most other years.

The ozone layer acts as a shield against ultraviolet radiation, which can cause skin cancer. The ozone hole first appeared in the early 1980s and reached its maximum size of 29.6 million square kilometers in 2000. The Antarctic ozone hole has caused significant changes in the Southern Hemisphere surface climate during the summer, and will continue to appear at least until the middle of the century according to WMO/UNEP Scientific Assessment of Ozone Depletion: 2014 Assessment for Decision-Makers. Close observation of the ozone layer on a global scale (including that over the Antarctic region) remains important.

(Atsuya Kinoshita,
Ozone Layer Monitoring Center)

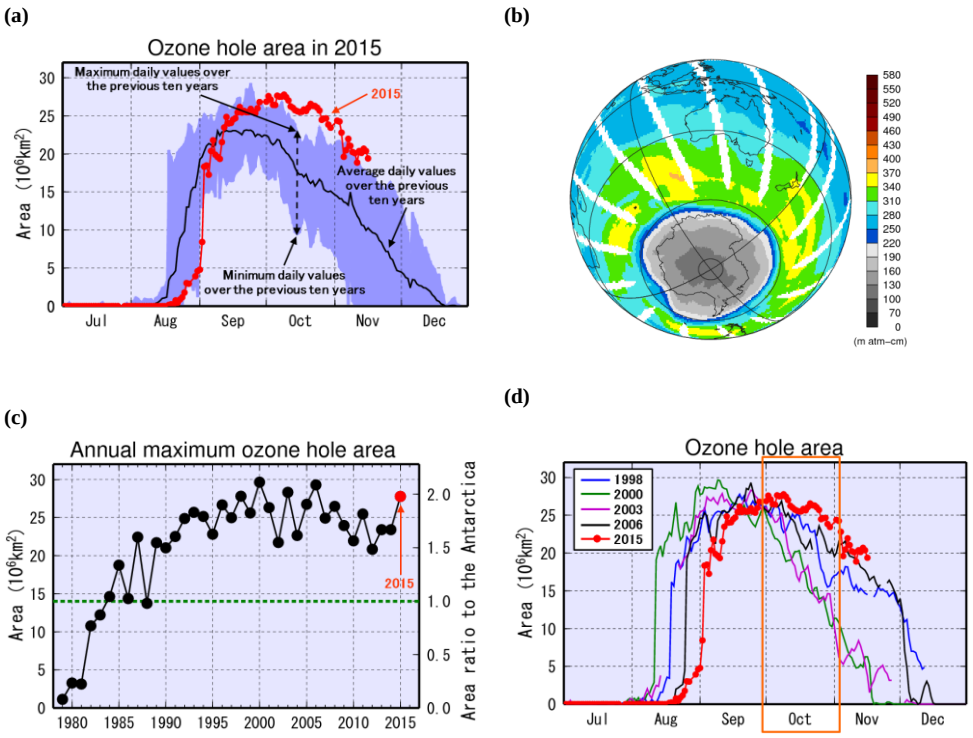

Figure 14 Characteristics of the Antarctic ozone hole in 2015

(a) Time-series representation of the daily ozone hole area for 2015 (red line) and the 2005–2014 average (black line). The blue shading area represents the range of daily minimum and daily maximum over the previous 10 years.

(b) Southern Hemisphere distribution of total ozone column on October 9, 2015, when the area of the ozone hole reached its maximum for the year. The grey shading shows ozone hole areas where the total ozone column value is 220 m atm-cm or less. White regions are domains where no satellite data were available.

(c) Time-series representation of the annual maximum ozone hole area. NASA TOMS/OMI and NOAA-TOVS satellite data are used in calculation of the area for 1979–2015. The green line indicates the overall area of the Antarctic (1.39×10^7 km^2). The left axis shows the maximum ozone hole area in units of 10^6 km^2, and the right axis shows its ratio to the area of Antarctica itself.

(d) Time-series representation of the daily ozone hole area for the five years with the largest annual maximum ozone hole areas since 1979 (1998 (blue line), 2000 (green line), 2003 (purple line), 2006 (black line) and 2015 (red line)). The time series representation of October in each year is shown within the orange frame.

Upgrade of TCC's Interactive Tool for Analysis of the Climate System

In November 2015, TCC launched version 5 of its iTacs web-based application software.

iTacs stands for "Interactive Tool for Analysis of the Climate System," and was developed by JMA/TCC to assist National Meteorological and Hydrological Services (NMHSs). It can be accessed via a web browser and requires no additional software or plug-ins. Datasets available on iTacs include the Japanese 55-year reanalysis (JRA-55), outgoing longwave radiation (OLR) data provided by NOAA, and sea surface temperature (COBE-SST) data. To enable analysis of the characteristics and structure of climate systems, various types of charts (such as longitude-latitude maps, polar stereographic maps, cross sections and time-series representations) are supported. iTacs is also equipped with a variety of statistical functions, such as linear regression and correlation coefficients, EOF, SVD and FFT. It is useful both for climate system monitoring and for analyzing factors behind extreme climatic events.

In iTacs ver. 5, 30-year re-forecast (hindcast) datasets covering the period from 1981 to 2010 are additionally implemented with JMA's one-month ensemble prediction system. GrADS ver. 2.1 graphic software is built in, allowing the production of clear images with smooth anti-aliased lines. iTacs ver. 5 also provides more efficient connections between client PCs and web servers via a revamped web interface.

Although iTacs ver. 4 also currently remains available, support for this version will soon be terminated. Accordingly, users are encouraged to switch to ver. 5. The latest information on iTacs is provided at http://extreme.kishou.go.jp/tool/itacs-tcc2015/.

(Kazuto Takemura, Tokyo Climate Center)

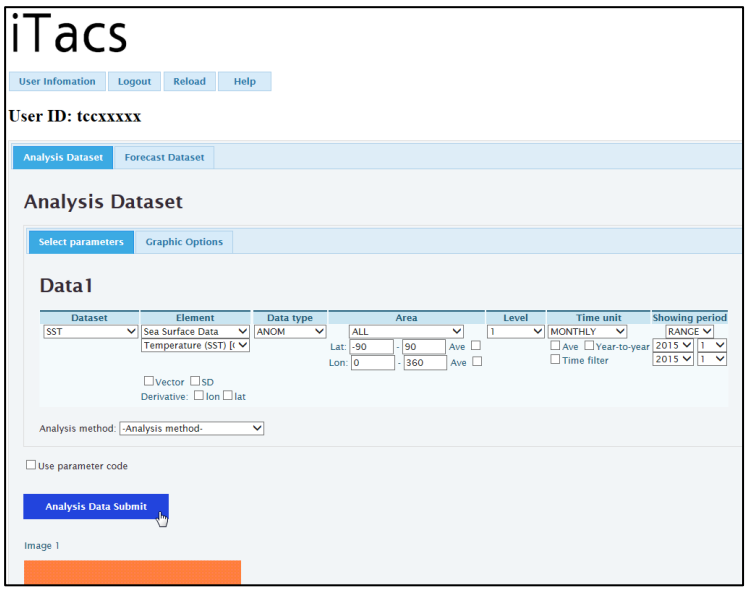

Figure 15 Top page layout of iTacs ver.5

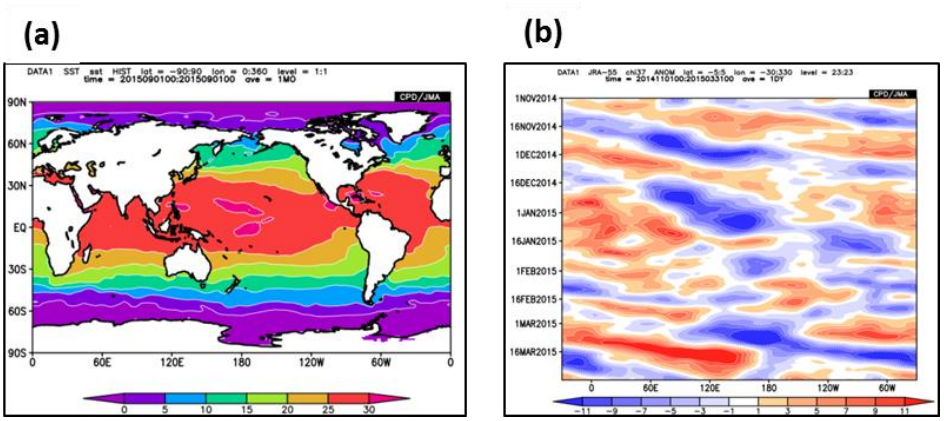

Figure 16 Example charts of iTacs ver.5

(a) SST in September 2015 and (b) longitude-time cross section of 5-day running mean 200-hPa velocity potential anomalies during the period from 1 November 2014 to 31 March 2015.

TCC Training Seminar on One-month Forecast

JMA's Tokyo Climate Center (TCC) assists National Meteorological and Hydrological Services (NMHSs) in improving their climate services. The Center's two major activities in this regard involve providing basic climate data and products to NMHSs through its website and assisting with capacity development at NMHSs in the Asia-Pacific region. TCC holds annual training seminars as part of capacity development activities related to its role as an RCC in the WMO RA II area. In addition to running annual training seminars, it arranges expert visits to and hosts visitors from NMHSs to support discussions on climate services and the effective transfer of technology.

In 2015, TCC held the Training Seminar on One-month Forecast from 16 to 20 November 2015 at JMA Headquarters in Tokyo. The event was attended by 15 experts from NMHSs in Bangladesh, Cambodia, Hong Kong (China), Indonesia, Lao People's Democratic Republic, Malaysia, Mongolia, Myanmar, Nepal, Pakistan, the Philippines, Singapore, Sri Lanka, Thailand and Viet Nam. The seminar focused on enhancing knowledge of one-month forecasts and related issues, and on improving individual countries' capacity for the generation of such forecasts. The course included lectures and practical exercises using data, products and a web-based application tool available on the TCC website as well as in-situ observation data brought by participants.

At the end of the seminar, all participants gave presentations on one-month forecast in their own countries and engaged in fruitful discussions with lecturers and participants. The content of the lectures is available on the TCC website at http://ds.data.jma.go.jp/tcc/tcc/library/library2015.html.

(Atsushi Goto, Tokyo Climate Center)

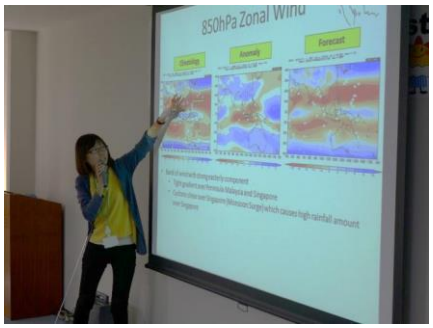

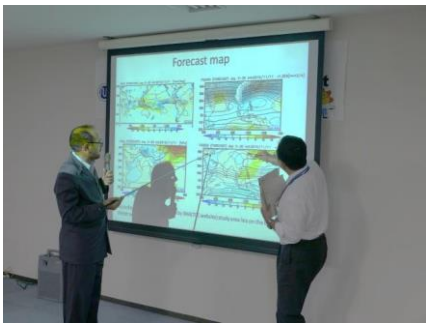

Any comments or inquiry on this newsletter and/or the TCC website would be much appreciated. Please e-mail to tcc@met.kishou.go.jp.

(Editors: Kazutoshi Onogi, Atsushi Goto and Yasushi Mochizuki)

Tokyo Climate Center (TCC), Japan Meteorological Agency
Address: 1-3-4 Otemachi, Chiyoda-ku, Tokyo 100-8122, Japan
TCC Website: http://ds.data.jma.go.jp/tcc/tcc/index.html